

Electronic Structure of Gadolinium and Dysprosium Using Compton Scattering Technique

Shabha Khera*, Narayan Lal Heda, Sonal Mathur, and Babu Lal Ahuja

Department of Physics, University College of Science, M. L. Sukhadia University, Udaipur - 313001 (Raj.), India

Reprint requests to Dr. B. L. A.; E-mail: blahuja@yahoo.com

Z. Naturforsch. **61a**, 299 – 305 (2006); received December 27, 2005

In this paper we present the first ever measured Compton profiles of polycrystalline gadolinium and dysprosium using 661.65 keV gamma-rays. The Compton data are compared with renormalized-free-atom (RFA) and free-electron model profiles. In both cases the RFA model (with $e^- - e^-$ correlation) gives a better agreement with the experiment. The hybridization effects of s-, p-, d-, and f-electrons are discussed, using the first derivatives of the Compton profiles. We also report the cohesive energy of both samples, computed from the RFA calculations. – PACS numbers: 13.60.F, 71.15.Nc, 78.70.-g, 78.70.Ck

Key words: Electron Momentum Density; Compton Scattering; Lanthanides; Cohesive Energy.

1. Introduction

Since the last three decades, Compton scattering has been exploited to measure the electron momentum distribution as a means of studying electronic behaviour in condensed matter [1]. The non-relativistic equations for conservation of energy and momentum lead to energy loss $\hbar(\omega_1 - \omega_2)$ as

$$\hbar(\omega_1 - \omega_2) = \frac{\hbar^2 k^2}{2m} + \frac{\hbar \vec{k} \cdot \vec{p}}{m}. \quad (1)$$

The second term in (1) is the Doppler term that arises as a result of the electron's motion and is a function of electron momentum \vec{p} . The conventional scattering vector \vec{k} is defined as $\vec{k} = \vec{k}_1 - \vec{k}_2$, where \vec{k}_1 and \vec{k}_2 are the incident and scattered photon wave vectors, respectively. The direction of \vec{k} is taken as z-axis of a set of Cartesian coordinates. The Doppler broadening of the Compton profile provides information about the electron momentum density distribution $n(\vec{p})$. The Compton profile, $J(p_z)$, is the probability distribution of the component momenta, p_z , viz.

$$J(p_z) = \iint n(p_x, p_y, p_z) dp_x dp_y. \quad (2)$$

One of the fundamental questions related to the lanthanides is whether their f-states are localized or

itinerant. Magnetic ordering is exhibited in heavy lanthanides namely Gd, Tb, Dy, Ho, Er and Tm at low temperatures. Particularly Gd is one of the four room temperature elemental ferromagnetic metals; the other three are Fe, Co and Ni. Due to this interesting behaviour of Gd, a considerable work, which mainly includes the band structure calculation, temperature-dependent magnetic ordering, photoemission, spin momentum density using magnetic Compton scattering, has been reported by several workers; see for example [2 – 10]. In case of Dy, most of the work is related to photoemission investigations, magnetic transitions using specific heat measurements, thermal effects at the first order phase transition, magnetic properties at high pressure etc.; see for example [11 – 14].

Recently, to investigate the electronic structure of lanthanides, our group has reported Compton profile data on Sm [15], Eu [16], Tb [17], Ho [18] and Yb [19], using a 20 Ci ^{137}Cs Compton spectrometer. We now present first experimental data for isotropic Compton profiles of Gd and Dy at intermediate momentum resolution (0.38 a.u.). The experimental Compton data and its first derivatives are compared with the renormalized-free-atom and free-electron model profiles. It is worth mentioning that the lanthanides present a special challenge to the crystal growers because of their chemical reactivity, which leads to difficulties in both the choice of containers and requirement of ultra high vacuum conditions. The attainment of ultra clean

* On leave from Department of Physics, Hindu College, Sonapat - 131001(Haryana), India.

Sample	Dimension	Exposure time (h)	Integrated counts (-10 to +10 a.u.)	Multiple scattering	Integrated BS contribution (-7 to +7 a.u.)	Normalization of profile (0 to 7.0 a.u.)
Gd	Ampoule diameter = 1.60 cm thickness = 0.40 cm, bulk density = 4.71 g/cm ³	148.36	1.3 · 10 ⁷	15.5%	0.18 e ⁻	24.32 e ⁻
Dy	Foil 1.2 cm × 1.2 cm, thickness = 0.10 cm, density = 8.54 g/cm ³	265.21	1.8 · 10 ⁷	8.7%	0.22 e ⁻	24.95 e ⁻

Table 1. Experimental parameters of the Compton profile measurements of Gd and Dy.

environmental conditions, which are necessary when handling high purity rare-earth metals at high temperatures, is clearly far more difficult to achieve during crystal growth. Therefore, due to difficulties in getting large size (about 13 mm diameter and 2 mm thickness) single crystals of Gd and Dy for Compton scattering experiments, we have undertaken the present measurements on polycrystalline samples. The units used for momentum densities are atomic units (a.u.). In this system $e = m = \hbar = 1$ and $c = 137.036$, and the unit of length is Bohr. The SI equivalent of 1 a.u. of momentum is $1.99 \cdot 10^{-24} \text{ kg m s}^{-1}$.

2. Experiment

The Compton profiles of Gd and Dy were measured using our 20 Ci ¹³⁷Cs Compton spectrometer; for details see [20, 21]. Collimated gamma-rays of 661.65 keV energy were allowed to fall normally on the sample, and the Compton-scattered gamma-rays were detected by an HPGe detector (Canberra, GLP0210) at a large scattering angle ($160^\circ \pm 0.6^\circ$). The details on both the samples and their measurements are given in Table 1. The raw Compton data were accumulated by a multichannel analyzer (Canberra, Accuspec B) with a channel width of 0.035 a.u. The overall momentum resolution (Gaussian FWHM) of the spectrometer was 0.38 a.u., which is much better than the previously achieved resolution (0.60 a.u.) using ²⁴¹Am Compton spectrometers. During the measurements, the electronic drift in the detection system was checked from time to time and was observed to be smaller than one channel (0.035 a.u.).

The true Compton profile was extracted from the energy distribution by the standard scheme of the War-

wick group [22], which involved subtraction of a background measured in the set up without a sample, deconvolution, correction for detector efficiency, corrections for photon absorption and for the Compton cross section, transformation of energy into the momentum scale, and normalization of the profile to the free-atom profile area. The instrumental resolution correction (deconvolution) was limited to stripping off the low energy tail from the data, therefore leaving the theoretical profile to be convoluted with the experimental resolution (Gaussian FWHM 0.38 a.u.). For both the samples, we have made a correction for multiple scattering by means of a Monte Carlo program developed by Felsteiner *et al.* [23]. In this program the ratio α of the number of multiple scattering events in the Compton profile to the total number of scattering events is calculated as a function of the sample material and dimensions, photon energy, beam geometry, etc. The effect of multiple scattering in both samples in the momentum region -10 to $+10$ a.u. is given in Table 1. The experimental Compton profile of Gd after various stages of data correction is shown in Figure 1. The spectral distribution of single, double and triple (almost negligible) scattered radiations for the same sample is shown in the inset of this figure. Further, as suggested by our group [24], we have also corrected the experimental profile for the bremsstrahlung (BS) background due to photo and Compton recoiled electrons liberated in the sample. As given in Table 1, the BS contribution in case of Dy was found to be higher than in case of Gd.

3. Theory

In the absence of band structure calculations, we have used the renormalized-free-atom (RFA)

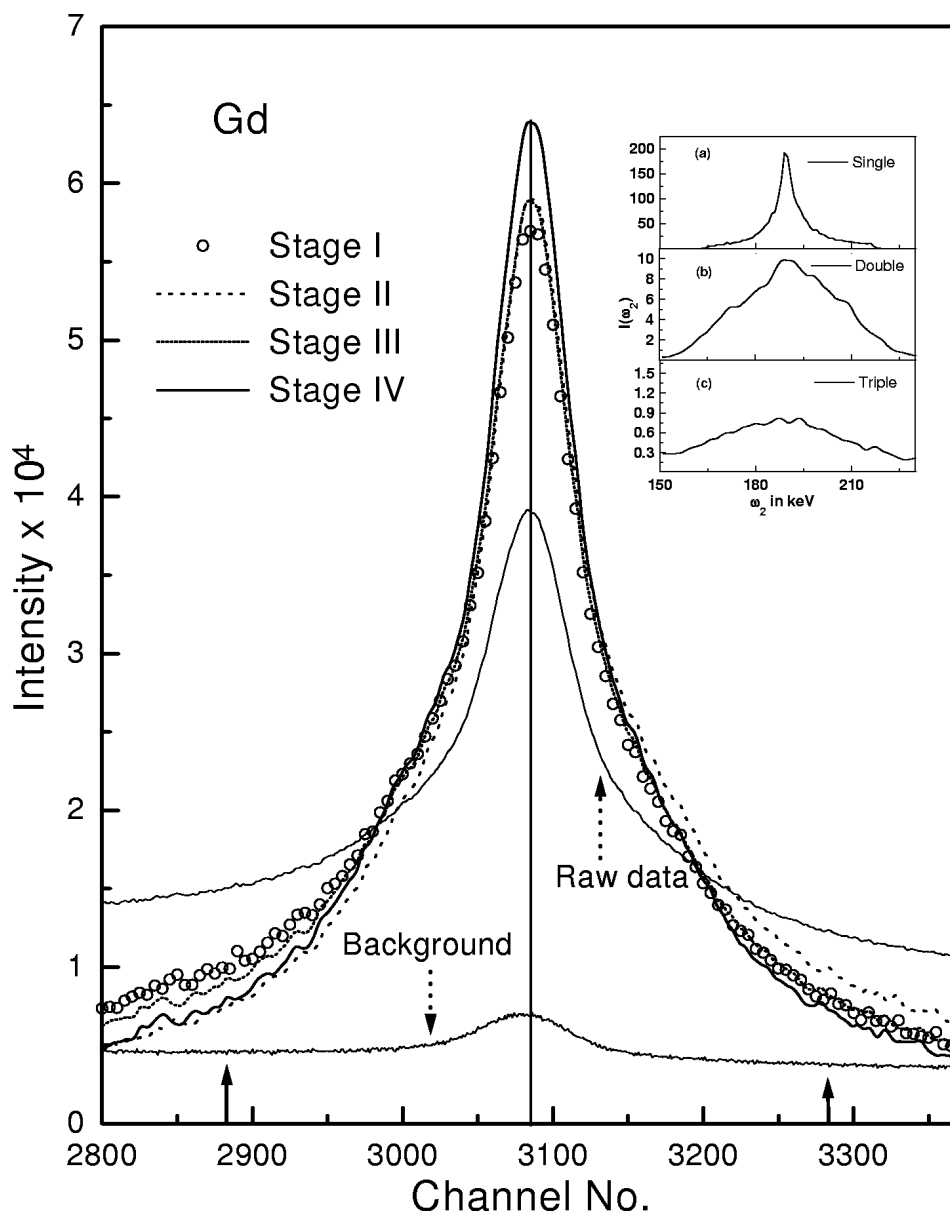


Fig. 1. Effect of various corrections during the extraction of true Compton profiles from the raw data of Gd. The shapes of data at various stages are: stage I, profile after background subtraction; stage II, profile after stage I, followed by partial deconvolution and detector efficiency correction; stage III, profile after stage II, followed by sample absorption and Compton scattering cross section correction; stage IV, profile after stage III, followed by correction for multiple scattering effects. Inset: spectral intensity distribution, $I(\omega_2)$, of (a) single, (b) double, and (c) triple scattered radiations simulated using Monte Carlo simulations.

model [25], which was found to be successful in the computation of Compton profiles of other lanthanides; see for example [15–19]. In this model, the atomic wave function was truncated at the Wigner-Seitz (WS) radius and renormalized to one per electron within the

WS sphere to preserve the charge neutrality. In this way the solid is constructed from individual atoms. In the case of Gd and Dy it was found that 43.9 and 38.5%, respectively, of the atomic 6s wave functions [26] were inside the WS spheres, whereas the

Table 2. The theoretical (unconvoluted) and experimental Compton profiles of Gd and Dy. In order to compare the theoretical profile with the respective experimental profile, the theoretical profile has to be convoluted with the momentum resolution function of the spectrometer (Gaussian FWHM 0.38 a.u.). Statistical error ($\pm \sigma$) is given at few points.

p_z in a.u.	$J(p_z)$ in e/a.u.							
	Gd				Dy			
	FE	RFA	RFA ($e^- - e^-$)	Expt.	FE	RFA	RFA ($e^- - e^-$)	Expt.
0.00	10.476	10.076	10.030	9.566 ± 0.028	10.183	9.950	9.903	9.300 ± 0.024
0.10	10.359	9.955	9.910	9.548	10.130	9.883	9.836	9.288
0.20	10.189	9.848	9.802	9.452	9.918	9.715	9.670	9.186
0.30	9.815	9.495	9.458	9.221	9.565	9.345	9.306	8.995
0.40	9.276	9.111	9.090	8.880	9.064	8.958	8.934	8.689
0.50	8.575	8.457	8.471	8.528	8.401	8.276	8.286	8.359
0.60	7.696	7.825	7.903	8.111	7.594	7.653	7.723	8.048
0.70	7.120	7.315	7.378	7.682	6.994	7.100	7.173	7.701
0.80	6.792	6.978	6.986	7.260	6.731	6.827	6.839	7.296
1.00	6.127	6.284	6.284	6.502 ± 0.022	6.151	6.238	6.238	6.465 ± 0.018
1.20	5.513	5.631	5.631	5.718	5.604	5.637	5.637	5.781
1.40	5.000	5.079	5.079	5.174	5.137	5.189	5.189	5.294
1.60	4.595	4.641	4.641	4.742	4.760	4.796	4.796	4.818
1.80	4.281	4.308	4.308	4.400	4.455	4.479	4.479	4.485
2.00	4.044	4.063	4.063	4.125 ± 0.016	4.182	4.243	4.243	4.207 ± 0.013
3.00	3.155	3.159	3.159	3.094 ± 0.013	3.328	3.331	3.331	3.296 ± 0.011
4.00	2.328	2.328	2.328	2.320 ± 0.011	2.490	2.489	2.489	2.445 ± 0.008
5.00	1.699	1.699	1.699	1.677 ± 0.008	1.830	1.830	1.830	1.825 ± 0.006
6.00	1.299	1.300	1.300	1.299 ± 0.007	1.390	1.390	1.390	1.413 ± 0.005
7.00	1.050	1.050	1.050	1.066 ± 0.006	1.100	1.099	1.099	1.098 ± 0.004

4f wave functions were found to be almost confined within the respective spheres. In case of Gd, about 90% of the 5d free atom wave function was within the WS sphere, thereby neglecting the renormalization effects. Therefore, 4f electrons of both lanthanides and 5d electrons of Gd were not considered in the RFA scheme. In Fig. 2 we have plotted the free atom (FA) and the RFA wave functions for 6s electrons of Gd and Dy used in the present RFA calculations. The Compton profiles for 6s² electrons of both lanthanides were calculated from the Fourier transform of the respective RFA wave functions $\psi^{(c)}(\vec{K}_n)$. For the hcp structure, the momentum density $n(\vec{p})$ can be derived using the relation [25]

$$n(\vec{p}) = 2 \sum_{|\vec{p}-\vec{K}_n| \leq p_F} |\psi^{(c)}(\vec{K}_n)|^2 \langle 1 + \cos \vec{K}_n \vec{\tau} \rangle / 2, \quad (3)$$

where p_F is the Fermi momentum. The factor two comes from the summations over the spin and τ determines the position of an atom in the unit cell, which for the hcp structure has the components $a/2$, $2\sqrt{3}a$ and $c/2$. In the present calculations, 25 shortest reciprocal lattice vectors (\vec{K}_n) were considered to incorporate the crystalline effects. For both cases we have also computed the free electron (FE) theory based Compton profiles using the formulae given in [25], treating 6s² electrons as free.

Total Compton profiles were obtained by adding the free atom core contribution [Xe]4f⁷5d¹ for Gd and [Xe]4f¹⁰5d⁰ for Dy from the tables of Biggs et al. [27] to the respective 6s² electron profile. The effect of the $e^- - e^-$ correlation (which shifts the momentum density from below the p_F to above p_F) was also incorporated in the RFA based $J(p_z)$ using the approach of Das and Chaddah [28]. All the total theoretical profiles were normalized in the same way as the experimental ones given in Table 1.

4. Results and Discussion

In Table 2 we present the experimental Compton profiles of Gd and Dy together with the unconvoluted Compton profiles derived from the RFA (with and without incorporating the $e^- - e^-$ correlation effect) and the FE models. All theoretical and experimental $J(0)$ values of Gd are found to be higher than the respective values for Dy. To compare the theoretical profiles with the respective experimental profiles, all the theoretical profiles were convoluted with the instrumental function (Gaussian FWHM of 0.38 a.u.) of the experiment. Figure 3 depicts the differences (ΔJ) between the convoluted theory and the experiment for both lanthanides. As expected, the FE model based profiles give a poor agreement with the experiment,

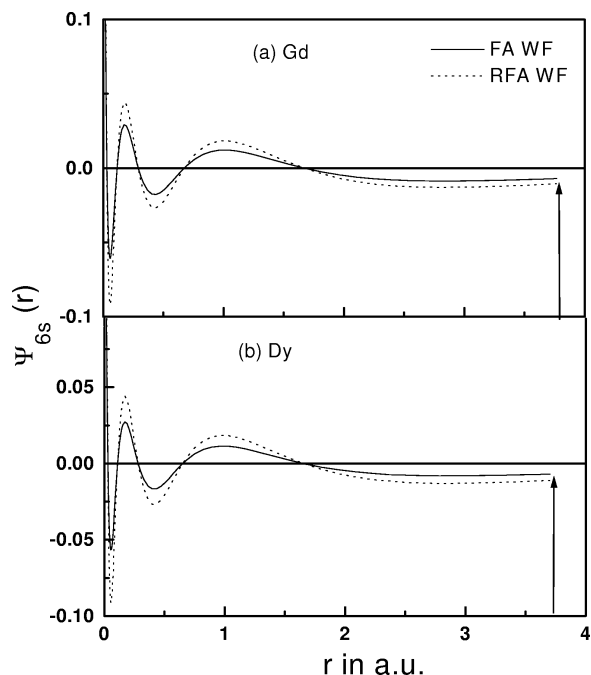


Fig. 2. Hartree-Fock-free-atom wave function (FAWF) and renormalized-free-atom wave function (RFAWF) for 6s electrons in (a) Gd and (b) Dy. The vertical arrows show the respective radius for the Wigner-Seitz sphere.

which may be due to unrealistic assumptions of the FE theory in case of Gd and Dy.

In both the cases, the RFA model profile with the $e^- - e^-$ correlation gives a better agreement with the respective measurement, although in the low momentum region the RFA calculations (with and without electron correlation effect) overestimate the momentum density. The large deviations between the simple RFA model and the Compton measurements may be due to the negligence of hybridization effects of s-, p-, d-, f-electrons in our RFA calculations. In fact, due to the non-availability of free atom wave functions for 6p electrons and limitations in the truncation of 4f and 5d electrons, we could not model these electrons within the RFA scheme. We believe that the Compton profiles corresponding to the 5d and 6p electrons of both lanthanides are flatter than those corresponding to the 6s electrons. Therefore, a reasonable incorporation of 6p or 5d electrons in the evaluation of the total theoretical Compton profile will reduce the magnitude of the absolute theoretical profile in the low momentum region. Then it will lead to a better agreement between the theoretical and experimental momentum densities.

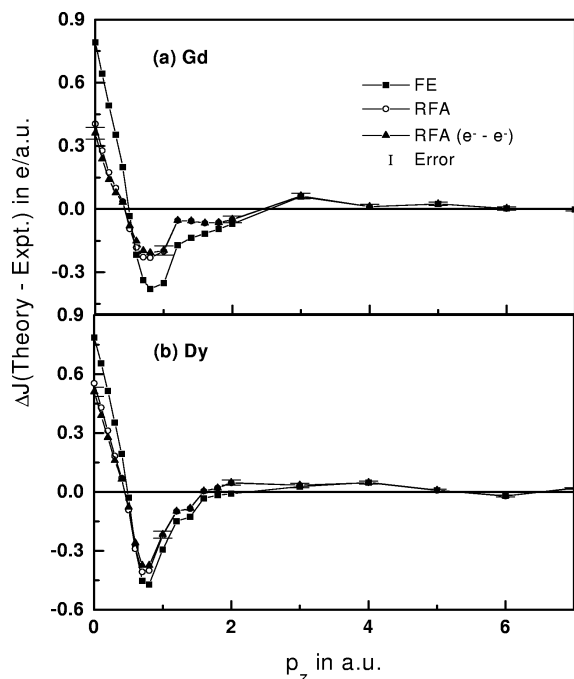


Fig. 3. Difference between the experimental and convoluted theoretical profiles for free-electron model (FE), RFA model, and RFA with $e^- - e^-$ correlation correction for (a) Gd and (b) Dy.

In order to derive additional information on the hybridization effects through Fermi surface related information, we have taken the first derivative $[dJ(p_z)/dp_z]$ of both the experimental Compton profiles and the FE model profiles computed for hypothetical 4, 6 and 8 electrons. It is worth mentioning that in the case of an FE profile for valence electrons (parabolic shape), the first minimum in the first derivative of the profile corresponds to the p_F . The first derivatives of the absolute experimental and the FE model profiles for both the lanthanides are shown in Figure 4. It is seen that the sharp drop in both the derivatives corresponding to the hypothetical 8 electrons based FE model profile occurs near a steep decrease of the experimental curve. Our FE based data show that there is a possibility of nearly eight electrons in the valence band of both lanthanides, which may only be due to spdf hybridization.

Now, coming to the cohesive properties, the cohesive energy E_{coh} is defined as the difference between the bulk and atomic total energies. The E_{coh} from the Compton profile data is given as [29]

$$E_{\text{coh}} = \int_0^{\infty} p_z^2 [J_S(p_z) - J_{\text{FA}}(p_z)] dp_z, \quad (4)$$

Table 3. Cohesive energy (E_{coh}) in eV for Gd and Dy along with the results of other investigations.

Sample	Our RFA	LMTO [31]		[32]
		GGA ^a	LDA ^b	
Gd	3.57	4.46	5.044	4.126
Dy	3.27	4.42	4.960	3.166

^a Generalized gradient approximation. ^b Local density approximation.

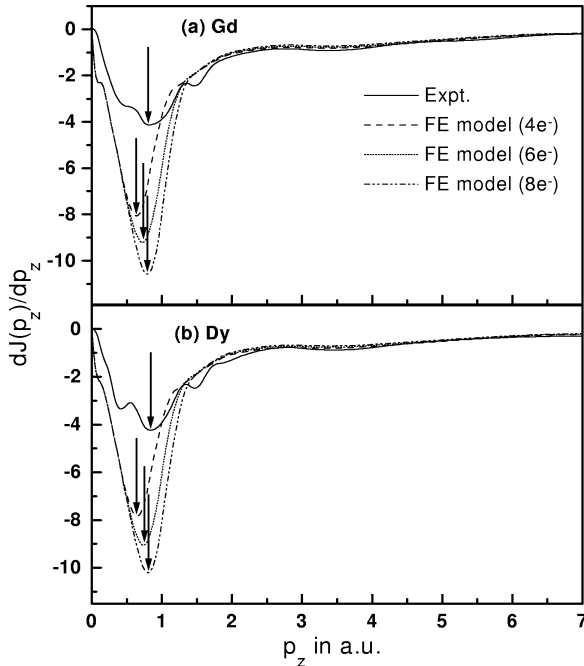


Fig. 4. The first derivatives of the convoluted total free-electron (FE) and experimental Compton profiles for (a) Gd and (b) Dy. In case of Gd, $[\text{Xe}]4f^{7-n}$ and $5d^{n+1}6s^2$ (where $n = 1, 3, 5$) are taken as core and valence band electrons, respectively; while for Dy the respective configurations are $[\text{Xe}]4f^{10-n}$ and $5d^n 6s^2$ (where $n = 2, 4, 6$).

where J_S and J_{FA} refer to the Compton profiles for the two states, namely solid and free atom. The values of

J_S were taken from the present RFA calculations, and those for J_{FA} from the free atom tables [27]. As reported by several workers, see, for example [29, 30], the computation of E_{coh} from the experimental Compton profile may be difficult due to the weighting of p_z^2 in (4) in the high momentum region. Therefore we have used only the RFA profiles for the calculations of cohesive energy of both lanthanides. In Table 3 we have listed the RFA based E_{coh} along with the available values of cohesive energies computed from the full potential LMTO with the local density approximation (LDA) and the generalized gradient approximation (GGA) [31]. For both lanthanides the RFA based cohesive energies are found to be smaller than the LMTO calculations [31], while these values are closer to the interpolation data of Johansson and Munck [32].

5. Conclusions

Isotropic Compton profiles of gadolinium and dysprosium have been interpreted in terms of free electron and renormalized-free-atom (with and without $e^- - e^-$ correlation) models. None of the models gives a reasonable agreement with the measurement. The first derivatives of both the profiles clearly suggest the hybridization effects of s-, p-, d- and f-electrons. The availability of an accurate band structure calculation, from which more precise theoretical Compton profiles can be computed, will be helpful to describe all the features of our measurements.

Acknowledgement

The authors would like to thank the Department of Science and Technology, New Delhi for financial support (grant No. SR/S2/CMP-16/2004). S. K. is thankful to the University Grant Commission, New Delhi for the award of a teacher research fellowship.

- [1] M. J. Cooper, Rep. Prog. Phys. **48**, 415 (1985) and references therein.
- [2] W.M. Temmerman, and P.A. Sterne, J. Phys.: Condensed Matter **2**, 5529 (1990).
- [3] N. Sakai, Y. Tanaka, F. Itoh, H. Sakurai, H. Kawata, and T. Iwazumi, J. Phys. Soc. Jpn. **60**, 1201 (1991); J. A. Duffy, J.E. McCarthy, S. B. Dugdale, V. Honkimaiki, M. J. Copper, M. A. Alam, T. Jarlborg, and S. B. Palmer, J. Phys.: Condensed Matter **10**, 10391 (1998).
- [4] D.M. Bylander and L. Kleinman, Phys. Rev. B **49**, 1608 (1994); D. M. Bylander and L. Kleinman, Phys. Rev. B **50**, 1363 (1994).
- [5] M. Heinemann and W.M. Temmerman, Phys. Rev. B **49**, 4348 (1994).
- [6] D. Li, P. A. Dowben, J.E. Ortega, and F.J. Himpsel, Phys. Rev. B **49**, 7734 (1994); B. Kim, A. B. Andrews, J. L. Erskina, K. J. Kim, and B. N. Harmon, Phys. Rev. Lett. **68**, 1931 (1992).
- [7] R. Ahuja, S. Auluck, B. Johansson, and M.S.S. Brooks, Phys. Rev. B **50**, 5147 (1994); O. Eriksson,

- R. Ahuja, A. Ormeci, J. Trygg, O. Hjortstam, P. Soderlind, B. Johansson, and J. M. Wills, *Phys. Rev. B* **52**, 4420 (1995).
- [8] C. Waldfried, D. N. McIlroy, and P. A. Downen, *J. Phys.: Condensed Matter* **9**, 10615 (1997) and references therein.
- [9] C. Santos, W. Nolting, and V. Eyert, *Phys. Rev. B* **69**, 214412 (2004).
- [10] I. Turek, J. Rusz, and M. Divis, *J. Magn. Magn. Mater.* **290–291**, 357 (2005).
- [11] P. O. Heden, H. Lofgren, and S. B. M. Hagstrom, *Phys. Rev. Lett.* **26**, 432 (1971).
- [12] K. D. Jayasuriya, S. J. Campbell, and A. M. Stewart, *Phys. Rev. B* **31**, 6032 (1985).
- [13] K. A. Gschneidner Jr., V. K. Pecharsky, and D. Fort, *Phys. Rev. Lett.* **78**, 4281 (1997).
- [14] D. D. Jackson, V. Malba, S. T. Weir, P. A. Baker, and Y. K. Vohra, *Phys. Rev. B* **71**, 184416 (2005) and references therein.
- [15] B. L. Ahuja, H. Malhotra, and M. Sharma, *Indian J. Phys.* **79**, 239 (2005).
- [16] B. L. Ahuja, H. Malhotra, and S. Mathur, *Z. Naturforsch.* **60a**, 512 (2005).
- [17] B. L. Ahuja, H. Malhotra, and M. Sharma, *Z. Naturforsch.* **59a**, 927 (2005).
- [18] B. L. Ahuja and M. Sharma, *Rad. Phys. and Chem.* **73**, 131 (2004).
- [19] B. L. Ahuja, and M. Sharma, *Phys. Status Solidi B* **241**, 2975 (2004).
- [20] B. L. Ahuja, M. Sharma, and S. Mathur, *Nucl. Inst. Meth. B* **244**, 419 (2006).
- [21] B. L. Ahuja and M. Sharma, *Pramana-Indian J. Phys.* **65**, 137 (2005).
- [22] D. N. Timms, Ph. D. Thesis, University of Warwick, England 1989; A. Andrejczuk, E. Zukowski, L. Dobrzynski, and M. J. Cooper, *Nucl. Inst. Meth. A* **337**, 133 (1993); M. J. Cooper, P. E. Mijnarends, N. Shiotani, N. Sakai, and A. Bansil, *X-Ray Compton Scattering*, Oxford Science Publications, New York 2004.
- [23] J. Felsteiner, P. Pattison, and M. J. Cooper, *Phil. Mag.* **30**, 537 (1974).
- [24] S. Mathur and B. L. Ahuja, *Phys. Lett. A* **335**, 245 (2004).
- [25] K. F. Berggren, S. Manninen, and T. Paakkari, *Phys. Rev. B* **8**, 2516 (1973); B. L. Ahuja, B. K. Sharma, and O. Aikala, *Pramana-Indian J. Phys.* **29**, 313 (1987).
- [26] F. Herman and S. Skillman, *Atomic Structure Calculations*, Prentice-Hall Inc., Englewood Cliffs, N.J. 1963.
- [27] F. Biggs, L. B. Mendelsohn, and J. B. Mann, *At. Data Nucl. Data Tables* **16**, 201 (1975).
- [28] G. P. Das and P. Chaddah, *Solid State Commun.* **45**, 607 (1983).
- [29] R. S. Holt and M. J. Cooper, *Phil. Mag. B* **41**, 117 (1980).
- [30] U. Mittal, B. K. Sharma, F. M. Mohammad, and B. L. Ahuja, *Phys. Rev. B* **38**, 12208 (1988).
- [31] A. Delin, L. Fast, O. Eriksson, and B. Johansson, *J. Alloys Compds.* **275–277**, 472 (1998).
- [32] B. Johansson and P. Munck, *J. Less-Common Met.* **100**, 49 (1984); B. Johansson, *Phys. Rev. B* **20**, 1315 (1979).